

October 31, 2018

## Nonlinear tube waves in permeable formations: Difference frequency generation

Yaroslav Tserkovnyak

Harvard University, Lyman Laboratory of Physics, Cambridge, Massachusetts 02138

David Linton Johnson

Schlumberger-Doll Research, Old Quarry Road, Ridgefield, Connecticut 06877-4108

**Abstract.** We extend earlier work on nonlinear tube wave propagation in permeable formations to study, analytically and numerically, the generation and propagation of a difference frequency,  $\Delta\omega = \omega_1 - \omega_2$ , due to an initial pulse consisting of carrier frequencies  $\omega_1$  and  $\omega_2$ . Tube waves in permeable formations have very significant linear dispersion/attenuation, which is specifically addressed here. We find that the difference frequency is predicted to be rather easily measurable with existing techniques and could yield useful information about formation nonlinear properties.

### Introduction

A tube wave is an acoustic normal mode in which the energy is confined to the vicinity of a fluid-filled cylinder within an elastic solid. From a practical point of view it is generally the dominant signal which appears in a typical borehole-logging measurement and thus it is important in a variety of contexts in the search for hydrocarbon sources.

One of these contexts lies in the fact that the tube wave may couple to fluid flow within the rock formation if the latter is permeable. The linearized tube wave propagation in this regime has been extensively studied both theoretically and experimentally [Winkler, *et al.*, 1989] (see also [Pampuri, *et al.*, 1998] and references therein). In the present article, we use a model of the tube wave due to [Liu and Johnson, 1997]. According to

the model, the fluid in the borehole is separated from the porous formation by an elastic membrane (mudcake) of finite thickness. As a tube wave propagates, the membrane flexes in and out of the pores, thus forcing the fluid to flow through the formation. This leads to the coupling between the tube wave and the acoustic slow wave in the formation, which in turn leads to attenuation and dispersion of the tube waves. In formations of moderate to large permeability, this mechanism is the largest known source of attenuation/dispersion of the tube wave and is the reason why it is specifically considered in the present article.

Quite apart from this effect it is also known that sedimentary rocks have very large coefficients of nonlinearity and so [Johnson, *et al.*, 1994] developed a theory for nonlinear tube waves neglecting the effects of the permeable formation. Later, [Johnson, 1999] combined this theory with the linearized theory of [Liu and Johnson, 1997] to describe a situation when the two effects are simultaneously present. As a numerical demonstration of the theory, [Johnson, 1999] considered the propagation of a narrow-banded (long duration) pulse consisting of a single carrier frequency. He showed that for realistic system parameters, the main signal (the fundamental) quickly decays, but before completely disappearing it generates a second harmonic and a low-frequency band (the “self-demodulated” pulse) both of which are due to the nonlinearity of the problem. The second harmonic decays even faster than the carrier, with the result that the self-demodulated pulse eventually dominates the entire signal at large enough distances.

Because the second harmonic decays so fast, often it is advantageous to determine nonlinear characteristics by using pulses which consist of two different carrier frequencies,  $\omega_1$  and  $\omega_2$ . In addition to the second harmonics (above) nonlinear effects lead to the generation of a signal centered around the difference frequency  $\Delta\omega = \omega_1 - \omega_2$ . This component may be reasonably energetic while at the same time it is not attenuated as much as either second harmonic, or even as much as either carrier frequency. Thus, in this article we are motivated to consider the propagation of two narrow-banded pulses whose frequency separation  $\Delta\omega$  is, say, 10% of the central frequency. Moreover, because  $\Delta\omega$  is not that different from  $\omega_{1,2}$ , it is often possible to measure its amplitude with the same acoustic transducers as for the fundamental.

The organization of the article is as follows. First, we review the theory and derive analytical results for the nonlinear propagation of a pulse consisting of two different frequencies. We derive an approximation for

the propagation of the entire signal and we find an analytical form for the energy of the band with frequency  $\Delta\omega$ . Next, we report results of numerical calculations for a few different parameter sets and we show a good agreement between our analytical and our numerical results. In the last section, we make a brief summary of our work.

## Theory

The dispersion and attenuation of the linear tube wave propagation has been studied in [Liu and Johnson, 1997]. To simplify our discussion we use an approximate form of the dispersion relation from [Johnson, 1999]:

$$k_z(\omega) = \omega \left[ S_\infty + \tilde{\Theta}(\omega) \right], \quad (1)$$

where  $k_z$  is the wave vector along z-direction (the tube axis),  $\omega$  is the angular frequency of the wave,  $S_\infty$  is the slowness at infinite frequency and  $\tilde{\Theta}$  is given by

$$\tilde{\Theta}(\omega) = \frac{\rho_f}{S_\infty b [W_{mc} + W_p(\omega)]}. \quad (2)$$

Here,  $\rho_f$  is the density of the borehole fluid,  $b$  is the borehole radius,  $W_{mc}$  is the mudcake membrane stiffness defined in [Liu and Johnson, 1997], and  $W_p$  characterizes permeability effects.  $W_p$  depends on the borehole fluid viscosity,  $\eta$ , formation permeability,  $\kappa$ , and the diffusivity of the slow wave

$$C_D = \frac{\kappa K_f^*}{\eta \phi} \quad (3)$$

through the equation

$$W_p(\omega) = -\frac{\eta C_D k_{SI} H_0^{(1)}(k_{SI} b)}{\kappa H_1^{(1)}(k_{SI} b)}. \quad (4)$$

Here,  $k_{SI} = \sqrt{\omega/C_D}$  is the wave vector of the slow-compressional wave and  $H_{0,1}^{(1)}$  are Hankel functions.

Tube waves in nonlinear hyperelastic and impermeable formations have been studied in [Johnson, *et al.*, 1994]. In [Johnson, 1999] the effects of linear attenuation/dispersion and nonlinearity have been combined to obtain an approximate equation of motion for tube wave propagation in a realistic borehole. In the retarded time frame  $\tau = t - S_\infty z$  this equation is

$$\frac{\partial p(z, \tau)}{\partial z} + \frac{\partial F(z, \tau)}{\partial \tau} - \frac{\beta S_\infty^3}{2\rho_f} \frac{\partial p^2(z, \tau)}{\partial \tau} = 0, \quad (5)$$

where  $p$  is the pressure,  $\beta$  is a dimensionless parameter defined in [Johnson, 1999]. The function  $F(z, \tau)$  is most simply related to the acoustic pressure in the Fourier transform domain:

$$\tilde{F}(z, \omega) = \tilde{\Theta}(\omega) \tilde{p}(z, \omega). \quad (6)$$

After performing the Fourier transform of Eq. (5), one obtains

$$\left( \frac{\partial}{\partial z} - \imath q(\omega) \right) \tilde{p}(z, \omega) + \frac{\imath \omega \beta S_\infty^3}{2 \rho_f} \tilde{p}^2(z, \omega) = 0, \quad (7)$$

where

$$q(\omega) = \omega \tilde{\Theta}(\omega) \quad (8)$$

is the reduced wave number. In Eq. (7),  $\tilde{p}^2(z, \omega)$  is the Fourier transform of the square of  $p(z, \tau)$  (*not* the square of the Fourier transform).

In [Johnson, 1999], Eq. (7) has been used to study the generation of the second harmonic as well as that of a low-frequency self-demodulated signal in a situation in which initially the pressure is a narrow band/long duration pulse centered on the frequency,  $\omega_1$ . In the present article we consider a situation when two narrow-banded pulses are initially present. As discussed in the Introduction, for practical relevance we will take the difference in the pulse frequencies  $\Delta\omega$  to be 10% of the central frequency  $\omega'$ . The initial signal is given by

$$p(z = 0, \tau) = E_1(\tau) \sin[\omega_1 \tau + \phi_1] + E_2(\tau) \sin[\omega_2 \tau + \phi_2]. \quad (9)$$

Here,  $E_i(\tau)$  are the envelope functions,  $\omega_1 \equiv \omega' + \Delta\omega/2$  and  $\omega_2 \equiv \omega' - \Delta\omega/2$ . For the numerical demonstration of the next section, we take the same envelope functions as in [Johnson, 1999]:

$$E_1(\tau) = E_2(\tau) = \frac{1}{2} P_0 \exp \left[ -(\tau/T_W)^{10} \right]. \quad (10)$$

By setting  $\omega_1 = \omega_2$  and  $\phi_1 = \phi_2$  in Eq. (9) one recovers the pulse considered in [Johnson, 1999]. In all three parameter sets used for the numerical calculations in the present article (see Table I), we take  $\Delta\omega/\omega' = 0.1$  and  $\omega' \times T_W = 125\pi$  so that initially the different signals we consider all “look” the same.

There are two characteristic distances relevant to the problem: the decay length of the linearized theory,  $Z_{\text{att}} = 1/\gamma(\omega')$ , where

$$\gamma(\omega) = \omega \Im \left[ \tilde{\Theta}(\omega) \right], \quad (11)$$

and the distance over which a shock front would develop, in the absence of attenuation. The latter is found in [Hamilton and Blackstock, 1998] to be

$$Z_{\text{shock}} = \frac{\rho_f}{\beta S_\infty^3 \omega' P_0}. \quad (12)$$

The Gol'dberg number

$$\Gamma = Z_{\text{att}}/Z_{\text{shock}} \quad (13)$$

measures the importance of nonlinear effects relative to the linear. In the three parameter sets (Table I), the amplitude  $P_0$  is chosen so that  $\Gamma = 0.21$ , i.e. the nonlinear effects are significant, but overall pulse propagation is dominated by linear dispersion/attenuation.

For  $\Gamma \ll 1$ , the nonlinear effects can be ignored to a first approximation. Because, by assumption, the signal consists of two narrow-band pulses one has the usual result of linear acoustics:

$$\begin{aligned} p'(z, \tau) = & E_1(\tau - \Delta S_{g1}z) e^{-\gamma_1 z} \sin [\omega_1(\tau - \Delta S_{p1}z) + \phi_1] \\ & + E_2(\tau - \Delta S_{g2}z) e^{-\gamma_2 z} \sin [\omega_2(\tau - \Delta S_{p2}z) + \phi_2], \end{aligned} \quad (14)$$

where  $\Delta S_p$  ( $\Delta S_g$ ) is the additional phase (group) slowness relative to  $S_\infty$ :

$$\begin{aligned} \Delta S_p(\omega) &= \Re \left[ \tilde{\Theta}(\omega) \right], \\ \Delta S_g(\omega) &= \frac{d}{d\omega} \Re \left[ \omega \tilde{\Theta}(\omega) \right]. \end{aligned} \quad (15)$$

Throughout this paper, the subscripts 1 and 2 correspond to frequencies  $\omega_1$  and  $\omega_2$ , respectively. The physical meaning of Eq. (14) is transparent: The pulse envelope propagates with the group velocity and attenuates while each peak and trough travels with the phase velocity. If the envelope is broad enough, the relevant attenuation/dispersion quantities should be evaluated at the central frequency of the pulse.

If the Gol'dberg number  $\Gamma$  is small compared to unity but is not completely negligible, Eq. (14) still gives a reasonable approximation for the propagation of the original pulses but, because of the quadratic nonlinearity in Eq. (7), new frequency components will be generated which are centered around  $\omega = 2\omega_1, 2\omega_2, 0$  as well as those centered around  $\omega_1 - \omega_2$  and  $\omega_1 + \omega_2$ . Apart from a direct numerical solution of Eq.(7) one can develop a perturbation theory thereof:

$$p(z, \tau) = p'(z, \tau) + p_0(z, \tau) + p_\Delta(z, \tau) + p_{2\omega_1}(z, \tau) + p_{2\omega_2}(z, \tau) + p_{\omega_1+\omega_2}(z, \tau) + \dots \quad (16)$$

Here,  $p_0$  refers to the self-demodulated signal,  $p_\Delta$  refers to the signal whose bandwidth is centered around  $\Delta = \omega_1 - \omega_2$ , etc. By substitution of Eqs. (14) and (16) into Eq.(7) one can derive an approximate equation for the evolution of these nonlinearly generated components, even in the presence of significant linear dispersion and attenuation.

In this manner the generation of the second harmonic and of the self-demodulated signal has been studied in [Johnson, 1999]. In the present article we focus on the component centered around the frequency  $\Delta = \omega_1 - \omega_2$ . (The analytical expressions we derive for this mode, can easily be generalized to the  $\omega = \omega_1 + \omega_2$  case by redefining  $\omega_2 \rightarrow -\omega_2$ .) We obtain ( $\Delta\phi \equiv \phi_1 - \phi_2$ )

$$p_\Delta(z, \tau) = E_1(\tau - \Delta S_{g1}z)E_2(\tau - \Delta S_{g2}z) \frac{\Delta\omega\beta S_\infty^3}{2\rho_f} \times \Re \left[ e^{-i(\Delta\omega\tau + \Delta\phi)} \frac{e^{i(q_1 - q_2^*)z} - e^{i\Delta\omega z}}{q(\Delta\omega) - q_1 + q_2^*} \right]. \quad (17)$$

One is reminded that this equation is valid only for narrow-banded pulses ( $\Delta\omega \times T_W \gg 1$ ) and small nonlinear effects ( $\Gamma < 1$ ).

Next, we consider the energy of the carrier ( $\omega \approx \omega'$ ) band,  $\mathcal{E}'(z)$  as well as that of the band centered on the difference frequency  $\omega \approx \Delta\omega$ ,  $\mathcal{E}_\Delta(z)$ . We define them by

$$\mathcal{E}'(z) \equiv \int_{\omega'/2}^{3\omega'/2} |\tilde{p}(z, \omega)|^2 d\omega, \quad (18)$$

$$\mathcal{E}_\Delta(z) \equiv \int_{\Delta\omega/2}^{3\Delta\omega/2} |\tilde{p}(z, \omega)|^2 d\omega. \quad (19)$$

Using Parseval's theorem and Eqs. (14) and (17), one gets

$$\begin{aligned} \mathcal{E}'(z)/\pi &\approx \int_{-\infty}^{+\infty} |\tilde{p}'(z, \omega)|^2 d\omega \\ &= e^{-2\gamma_1 z} \int_{-\infty}^{+\infty} E_1^2(\tau) d\tau + e^{-2\gamma_2 z} \int_{-\infty}^{+\infty} E_2^2(\tau) d\tau \end{aligned} \quad (20)$$

and

$$\begin{aligned} \mathcal{E}_\Delta(z)/\pi &\approx \int_{-\infty}^{+\infty} |\tilde{p}_\Delta(z, \omega)|^2 d\omega \\ &= \left( \frac{\Delta\omega\beta S_\infty^3}{2\rho_f} \right)^2 \left| \frac{e^{i(q_1 - q_2^*)z} - e^{i\Delta\omega z}}{q(\Delta\omega) - q_1 + q_2^*} \right|^2 \times \int_{-\infty}^{+\infty} E_1^2(\tau - \Delta S_{g1}z)E_2^2(\tau - \Delta S_{g2}z) d\tau. \end{aligned} \quad (21)$$

In the special case that the two envelope functions are identical,  $E_1(\tau) \equiv E_2(\tau)$ , one can derive a simple analytic result for the nonlinearly generated signals centered around  $\Delta\omega$  as well as the self-demodulated signal centered around  $\omega = 0$ . For this, we rewrite the input signal (9) in the form

$$p(z = 0, \tau) = E'(\tau) \sin[\omega' \tau + \phi'], \quad (22)$$

where  $\phi' \equiv (\phi_1 + \phi_2)/2$  and

$$E'(\tau) = 2E_1(\tau) \cos[(\Delta\omega/2)\tau + \Delta\phi/2]. \quad (23)$$

$E'(\tau)$  is now viewed as a narrow-banded envelope function for the  $\omega'$  mode (assuming that  $\Delta\omega \ll \omega'$ ). As before, the total signal can be approximated by

$$p(z, \tau) \approx p_{[slow]}(z, \tau) + p'(z, \tau) \quad (24)$$

where  $p_{[slow]}(z, \tau) \equiv p_0(z, \tau) + p_\Delta(z, \tau)$  now includes both the self-demodulated component as well as the components centered around  $\Delta\omega$ . Within the context of the foregoing approximations it is given by

$$p_{[slow]}(z, \tau) = \frac{\beta S_\infty^3}{4\rho_f} \int_{-\infty}^{+\infty} \frac{-i\omega \tilde{E}'^2(\omega)}{i\omega \Delta S'_g - 2\gamma' - iq(\omega)} \times \left[ e^{(i\omega \Delta S'_g - 2\gamma')z} - e^{iq(\omega)z} \right] e^{-i\omega \tau} d\omega. \quad (25)$$

The primed quantities  $\Delta S'_g$  and  $\gamma'$  are evaluated at the frequency  $\omega'$ .

## Numerical Results

For the numerical calculations, we consider three parameter sets, {A, B, C}, which are listed in Table I. These parameters are identical to those considered in [Johnson, 1999], where the relevance of these parameters to realistic borehole properties is discussed. There is one change in that in this article we take  $T_W$  to be five times larger. This is done in order to make the band widths of the pulses so narrow that the  $\Delta\omega$  mode clearly separates from the rest of the low frequency signal.

In order to solve the equation of motion (7) we use the same Lax-Wendroff algorithm as in [Johnson, 1999] and the initial pulse (9) with envelope functions (10) and phases  $\phi_1 = \phi_2 = 0$ . Figs. (1), (2), and (3) show several snapshots of the pulse profile in both time and frequency domains for three parameter sets (Table I) A, B and C, respectively. Cases B and C have similar initial pulses, but differ somewhat in their dispersion relations, as can be

seen from the corresponding parameter sets in Table I. Sample A has a center frequency two orders of magnitude lower than samples B and C, and as a consequence, the relevant modes have much longer attenuation length  $Z_{\text{att}}$ .

It is pedagogically useful to first examine Fig. 3 in detail. Considering the left column of plots, one can trace an intuitively clear sequence of events: Initially, the signal is given by two sharp pulses separated by 10% frequency difference  $\Delta\omega$  (first row of plots). As this signal propagates through the borehole and gradually attenuates, modes centered at  $\omega \approx \Delta\omega$  are being generated (second row). They soon start to dominate the general shape of the pulse because they attenuate less than does the carrier (third row). Concomitantly,  $\omega \approx 0$  modes start to appear and give a significant “background” for the  $\Delta\omega$  signal (fourth row). In the end, all higher-frequency components decay and the completely self-demodulated signal  $\omega \approx 0$  contains most of the energy (fifth row). One has to be careful looking at the right column of the plots: The black profile of the first plot outlines an envelope Eq. (23) of the 10kHz signal, detailed structure of which can be seen only if we expand the time scale  $\tau$  (second and third plots). In order to examine the  $\Delta\omega \approx 100$ Hz components and the lower-frequency signal, we again show the entire signal in the last two plots. Although Eq. (24) is also plotted, it is indistinguishable from the results of the full numerical calculation. For large enough distance  $p(z, \tau)$  evolves to  $p_{[\text{slow}]}(z, \tau)$ , Eq. (25), as is indicated in the plot.

Qualitatively Fig. 1 and Fig. 2 look similar to Fig. 3. But in the case of sample A, because of the smaller attenuation, the  $\Delta\omega$  component does not demodulate completely even after propagating a distance of  $\sim 40$ km.

Next, for each of the three cases, A, B, and C, we calculate the energy of the  $\omega = \omega'$  band directly using Eq. (18) and also using Eq. (20). Similarly, we calculate the energy of the  $\omega = \Delta\omega$  band using Eq. (19) as well as Eq. (21). The results are plotted in Figs. 4, 5 and 6. One can compare Fig. 5 with Fig. 6 of [Johnson, 1999] which shows the energy of the second harmonic and the  $\omega = 0$  band for an almost monochromatic initial pulse and same system parameters. As can be intuitively expected, the  $\Delta\omega$  band is intermediate in both the maximal energy it gains and the distance it propagates, as compared to the lower-frequency band and the higher harmonics. The  $\Delta\omega$  component does not reach energies as high as the second harmonics do, but it propagates much further, still carrying a significant fraction of energy; it is  $\sim 55$ dB down from the initial carrier energy,  $\mathcal{E}'(z = 0)$ , in our examples. On the other hand, while the lower-frequency signal persists longer than the  $\Delta\omega$  modes, it is never as

energetic and it would be more difficult to measure even in principle.

The intersections of the solid and dashed curves in Figs. 4, 5, and 6 indicate the crossover region, where the  $\omega = \Delta\omega$  band starts dominating over the carrier band  $\omega = \omega'$ , as can be seen in Figs. 1, 2, and 3, respectively.

## Conclusions

We have used the theory of [Johnson, 1999] of tube wave propagation in permeable formations to describe nonlinear interaction of two narrow-banded pulses. The theory incorporates both nonlinear effects and a realistic model for dispersion/attenuation of tube waves. We have extended this previous work on the propagation of a single narrow-banded pulse to describe the generation and propagation of the  $\omega = \Delta\omega$  band when two different carrier frequencies are present in the initial pulse.

We have derived analytical results for the self-demodulated component, the  $\Delta\omega$  band, and the total signal in the regime of weak nonlinearity and they are in excellent agreement with an accurate numerical calculation using three different parameter sets. Specifically, we have studied the spectral content of the signal and demonstrated that the  $\Delta\omega$  band can have a potential application because of its long attenuation length and its relatively high energy content. Also, if  $\Delta\omega/\omega' \sim 0.1$ , as we consider here, there is a practical bonus as the same transducers used for the generation of the carrier signal can, presumably, be used for the detection of the  $\Delta\omega$  band.

**Acknowledgments.** This work was supported in part by the NSF grant DMR 99-81283.

## References

Hamilton, M. F., and Blackstock, D. T. (1998). *Nonlinear Acoustics*, (Academic, New York).

Johnson, D. L. (1999). "Nonlinear pulse propagation in arbitrary dispersive media: Tube waves in permeable formations," *J. Acoust. Soc. Am.* **105**, 3087-3096.

Johnson, D. L., Kostek, S., and Norris, A. N. (1994). "Nonlinear tube waves," *J. Acoust. Soc. Am.*, **96**, 1829-1843.

Liu, H.-L., and Johnson, D. L. (1997). "Effects of an elastic membrane on tube waves in permeable formations," *J. Acoust. Soc. Am.* **97**, 3322-3329.

Pampuri, F., Rovellini, M., Brie, A., and Fukushima, T., (1998). "Effective evaluation of fluid mobility from Stoneley waves using full Biot model inversion: Two case histories," in SPE Annual Technical Conference and Exhibition, Paper 49132, New Orleans (SPE, Richardson, TX, 1998).

Winkler, K. W., Liu, H.-L., and Johnson, D. L. (1989). "Permeability and borehole Stoneley waves: Comparison between experiment and theory," *Geophysics* **54**, 66-75.

---

**Table 1.** Values of input parameters for the calculation of tube wave characteristics.

Sample		A	B	C	
	$\phi$	0.30	0.30	0.30	
	$\eta$	0.01	0.01	0.01	poise
	$K_f^*$	2.25	2.25	2.25	GPa
	$b$	0.1	0.1	0.1	m
	$\rho_f$	1000.	1000.	1000.	kg/m <sup>3</sup>
Input	$S_\infty$	667.	667.	667.	$\mu\text{sec}/\text{m}$
parameters	$\beta$	50.5	50.5	50.5	
	$W_{\text{mc}}$	250.	250.	100.	GPa/m
	$\kappa$	2.	0.2	0.2	$\mu\text{m}^2$
	$\omega'/2\pi$	0.1	10.	10.	kHz
	$T_W$	625.	6.25	6.25	msec
	$P_0$	81.	80.	92.	kPa
<hr/>					
	$C$	15.	1.5	1.5	$\text{m}^2/\text{sec}$
	$Z_{\text{att}}$	278.	2.8	2.4	m
Calculated	$Z_{\text{shock}}$	1323.	13.4	11.6	m
quantities	$\Gamma = Z_{\text{att}}/Z_{\text{shock}}$	0.21	0.21	0.21	
	$\Delta S_p(\omega')$	55.9	6.8	6.9	$\mu\text{sec}/\text{m}$
	$\Delta S_g(\omega')$	52.7	3.5	3.5	$\mu\text{sec}/\text{m}$

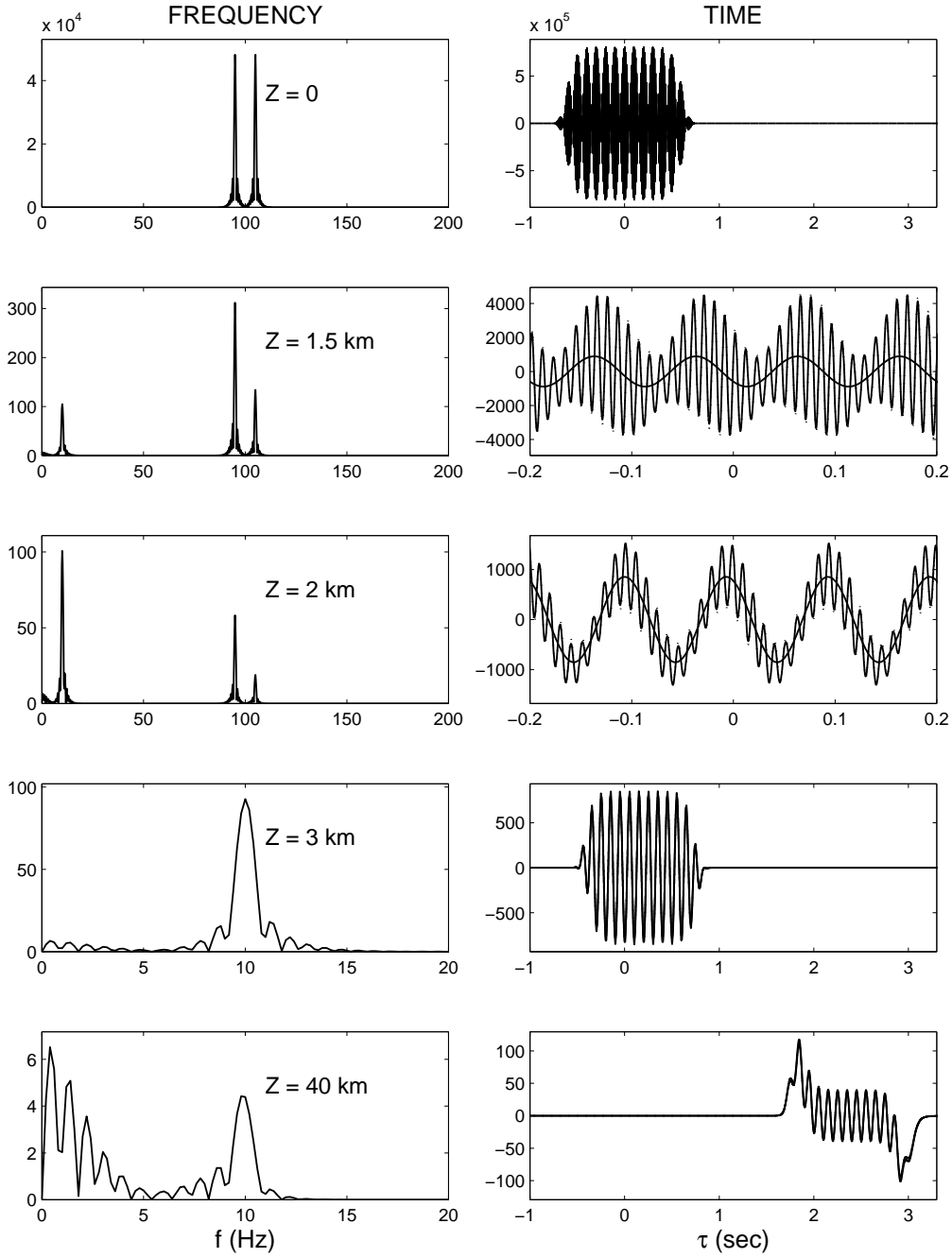


**Figure 1.** Calculated pulse evolution using parameter set A, from Table I. The right column is the signal in the time domain, the left is the frequency spectrum. Also shown as a solid line on the right is the analytical expression for the low-frequency pulse, Eq. (25), toward which the pulse evolves. Similarly, the analytical expression for the total signal, Eq. (24), is shown as a dotted line: It essentially overlies the numerically calculated signal. Notice the various changes of scale.

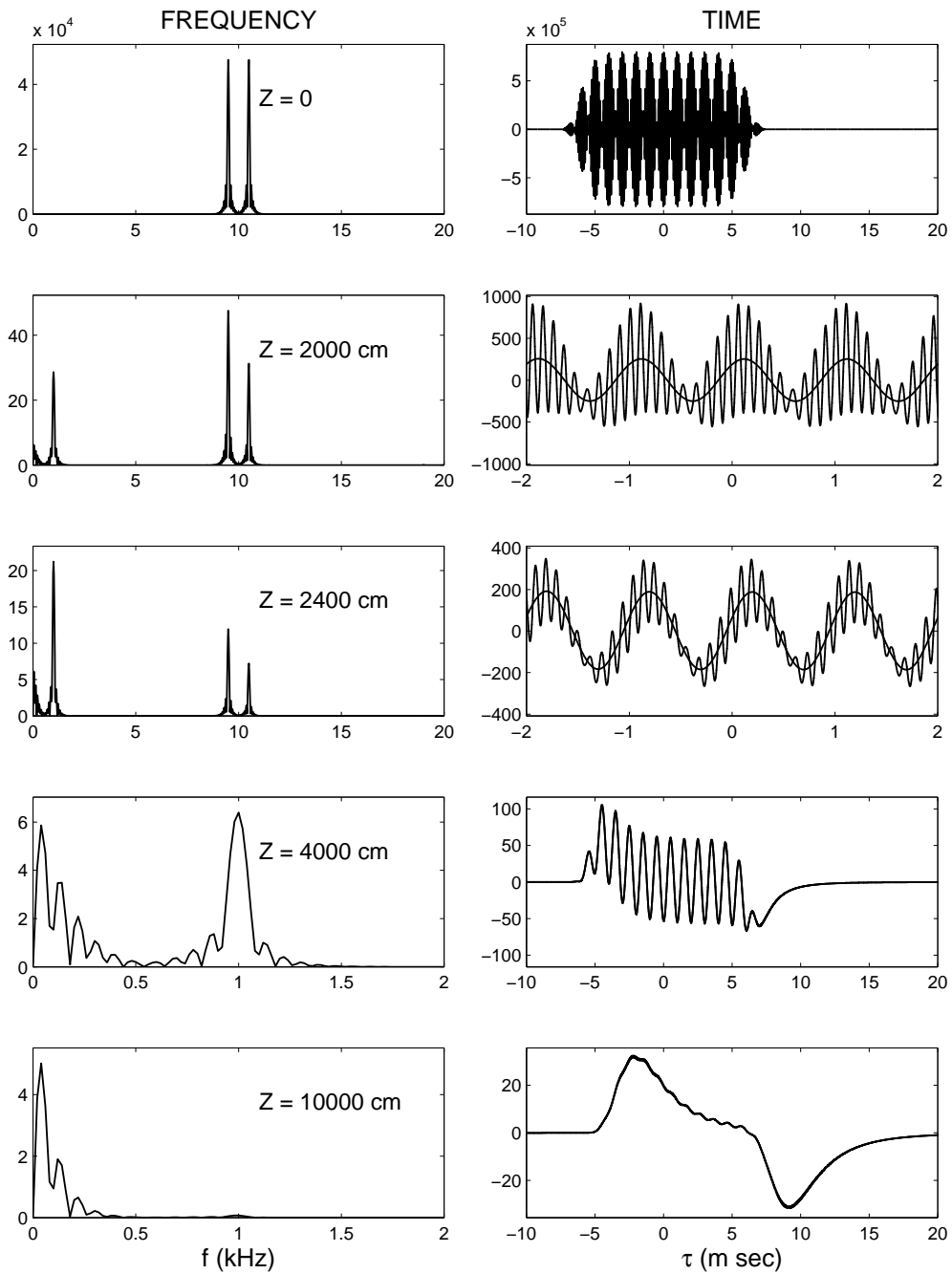


**Figure 2.** Calculated pulse evolution using parameter set B, from Table I. Same conventions as Fig. 1.

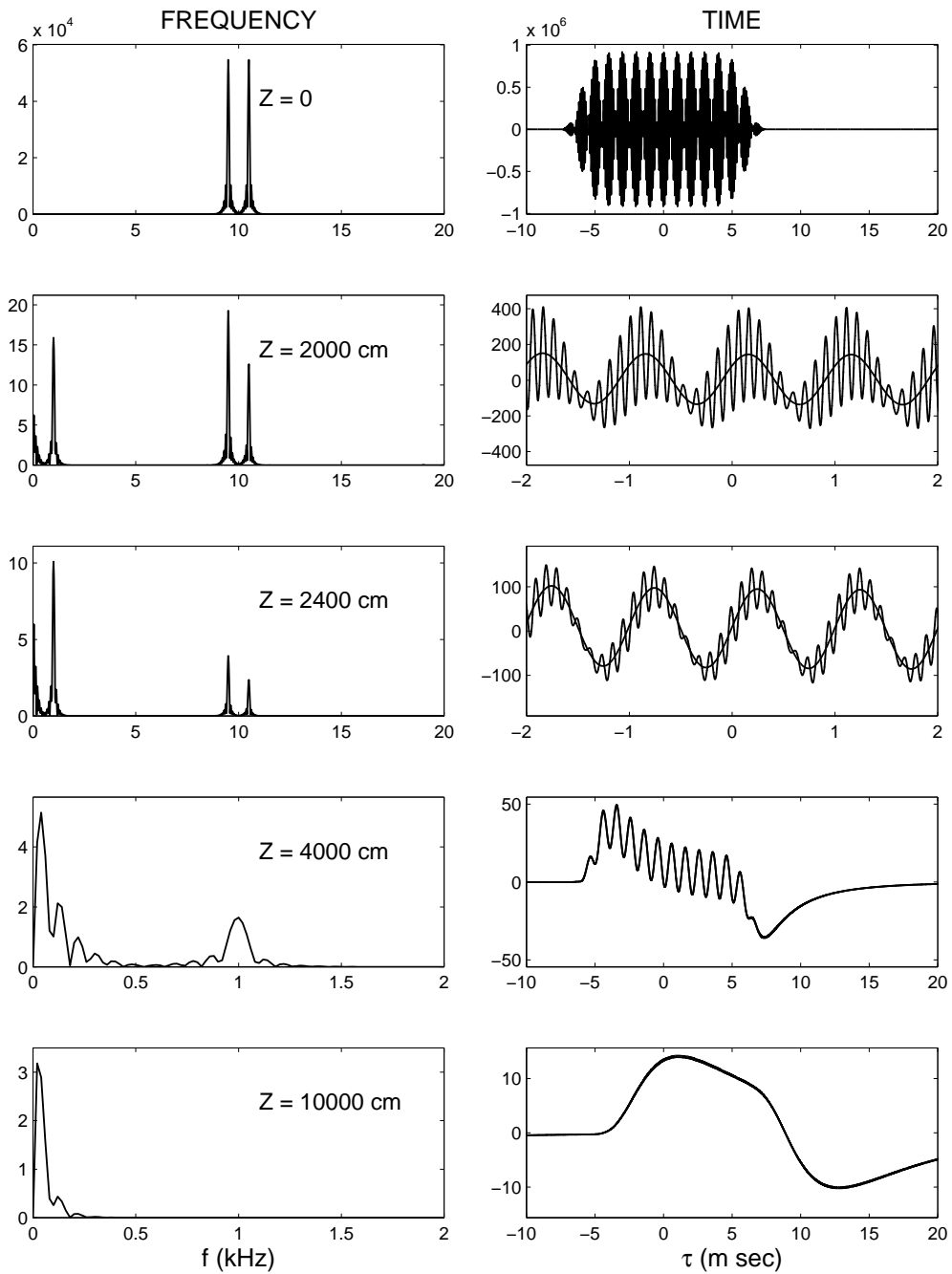


**Figure 3.** Calculated pulse evolution using parameter set C, from Table I. Same conventions as Fig. 1.

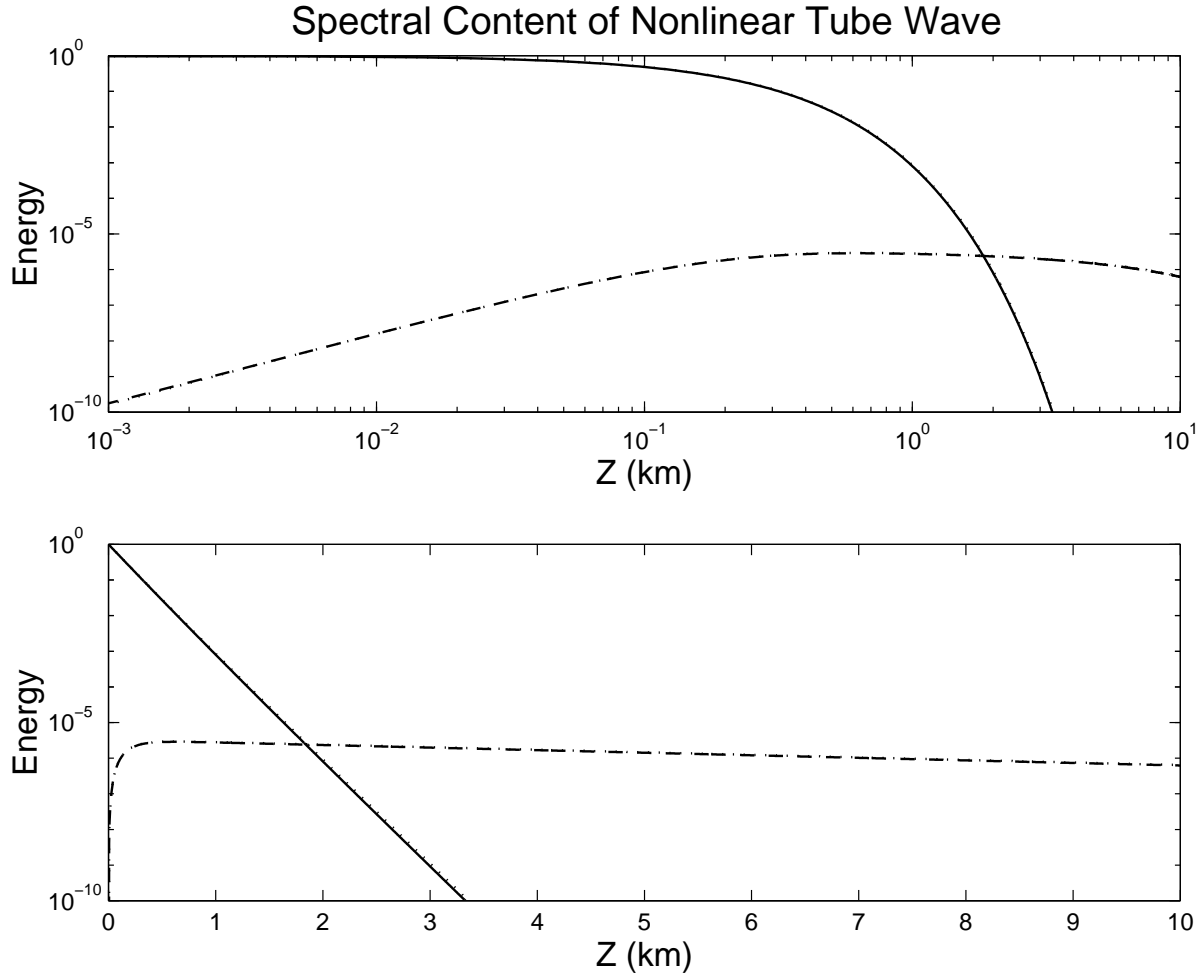


**Figure 4.** Numerically calculated values of the energy  $\mathcal{E}'(z)$  (solid line) and  $\mathcal{E}_\Delta(z)$  (dashed line) defined by Eqs. (18) and (19) for the waveforms of Fig. 1, sample A. Each curve has been normalized by the value of  $\mathcal{E}'(z = 0)$ . The data are shown in both log-log and semilog plots, in order to emphasize the short and long distance behavior, respectively. The dotted lines show the analytical expressions, Eqs. (20) and (21); the fact that they are almost indistinguishable from the numerically calculated curves is precisely the point.

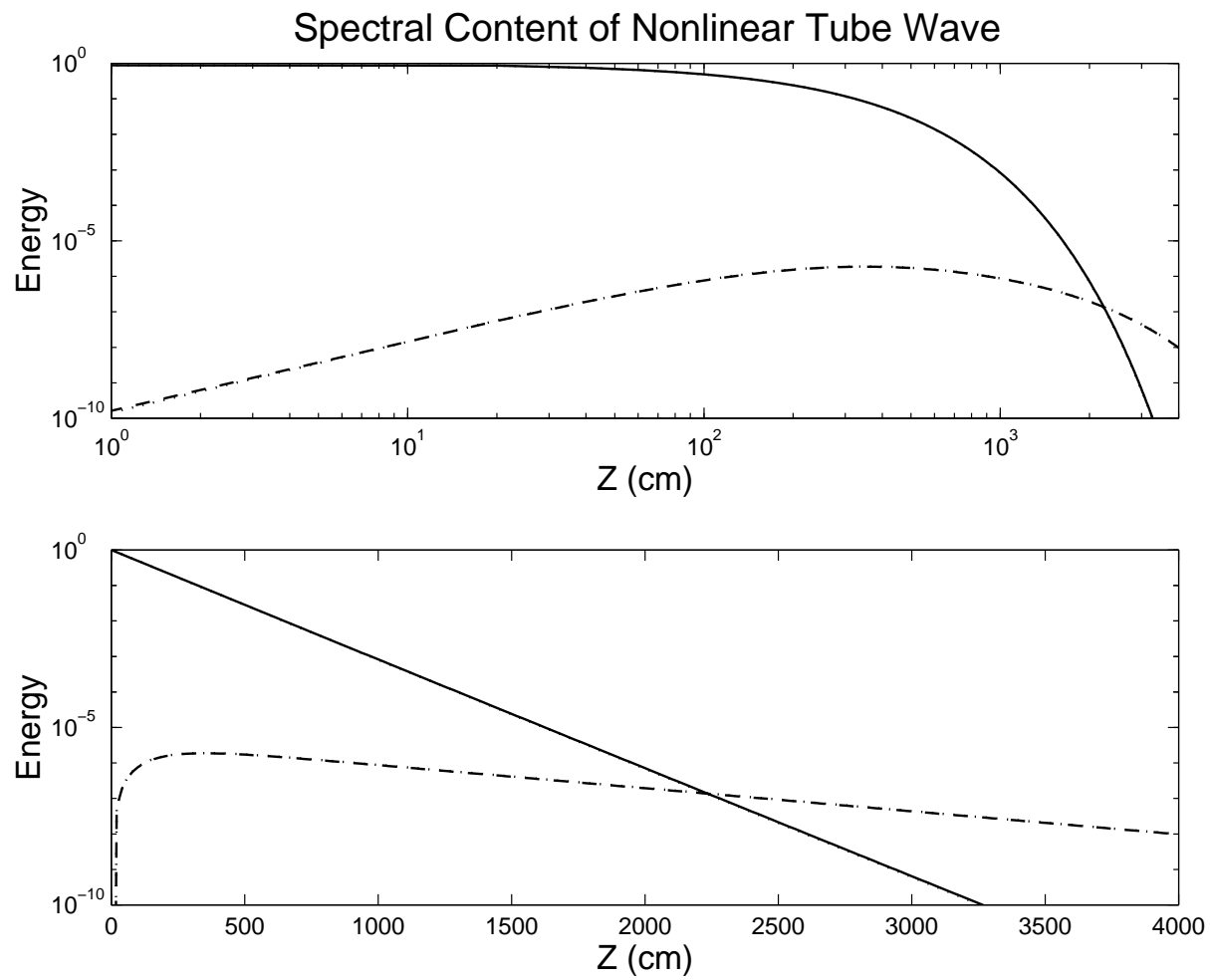


**Figure 5.** Numerically calculated values of the energy  $\mathcal{E}'(z)$  and  $\mathcal{E}_\Delta(z)$  for the waveforms of Fig. 2, sample B.

Same conventions as Fig. 4.

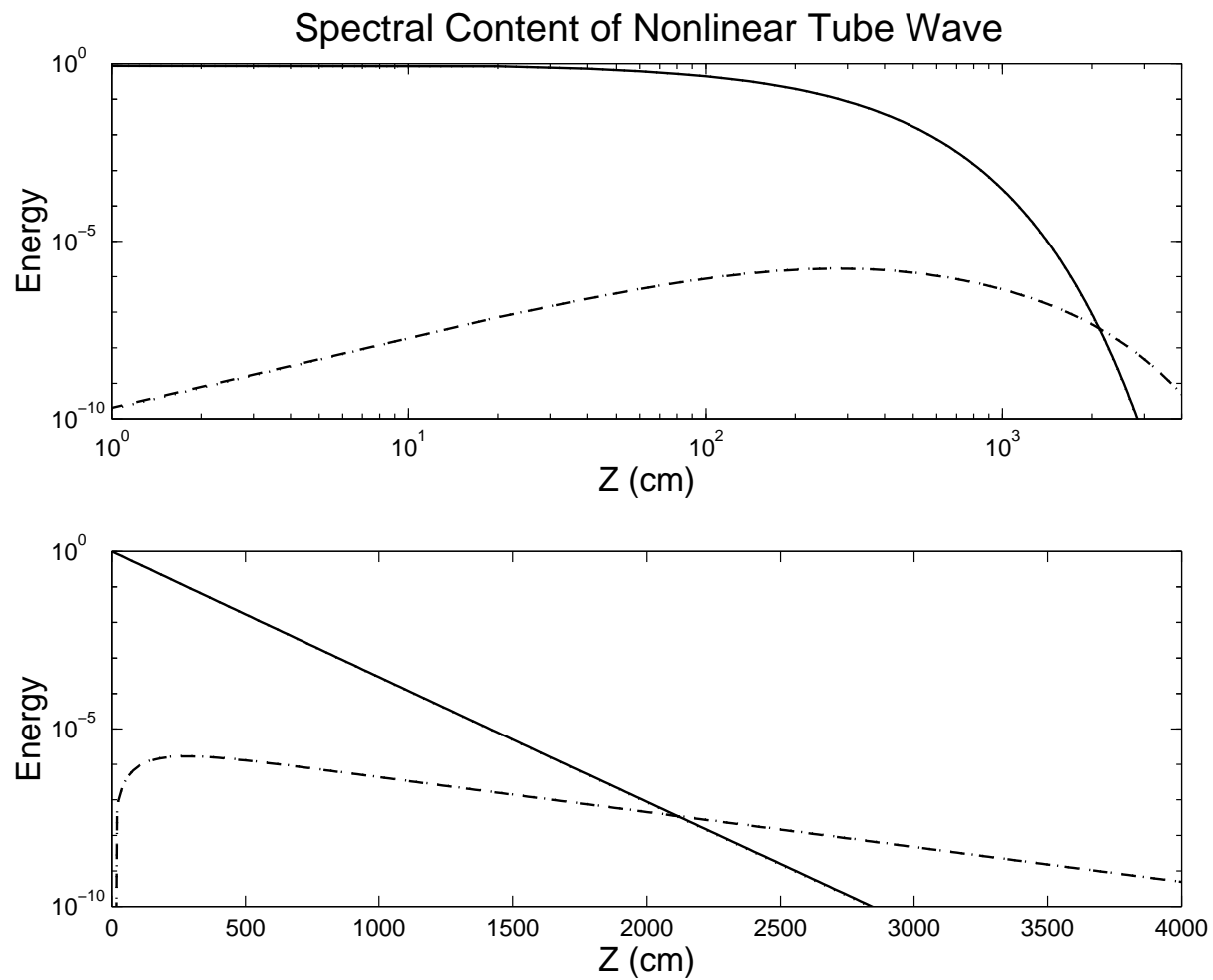


**Figure 6.** Numerically calculated values of the energy  $\mathcal{E}'(z)$  and  $\mathcal{E}_\Delta(z)$  for the waveforms of Fig. 3, sample C.

Same conventions as Fig. 4.